J Mater Sci (2025) 60:22662–22677

Composites & nanocomposites

Improving the thermal stability of fly ash-based geopolymer materials through cellulose nanocrystal reinforcement

Rishen Roopchund[1,*], Lanrewaju Fajimi[2], Naadhira Seedat[3], and Jerome Andrew[4]

[1] *Department of Chemical and Materials Engineering, College of Science, Engineering and Technology, University of South Africa, Roodepoort 1709, South Africa*
[2] *Department of Chemical Engineering, University of Johannesburg, Johannesburg, South Africa*
[3] *Department of Chemical Engineering, University of Pretoria, Private Bag X20, Hatfield, Pretoria 0028, South Africa*
[4] *Biorefinery Industry Development Facility, Council for Scientific and Industrial Research (CSIR), Durban, South Africa*

Received: 25 May 2025
Accepted: 1 October 2025
Published online: 3 November 2025

ABSTRACT

Prior to this study, the thermal stability of fly ash-based geopolymer (FAG) construction materials as a function of cellulose nanocrystal (CNC) concentration and the optimal CNC dosage leading to thermal stability have not been investigated. This study investigates the influence of CNC reinforcement and curing duration on the thermal stability of FAG geopolymer. A series of samples incorporating CNC dosages ranging from 0 to 1.86 wt.% were prepared and subjected to 24- and 48-h curing regimes to evaluate their thermal degradation behaviors. Thermogravimetric analysis (TGA) revealed that 24-h-cured samples exhibited steeper weight losses compared to 48-h-cured ones, particularly in the 100–600 ℃ range. This trend was attributed to incomplete stabilization of organics in shorter curing times. Among all dosages, the 48-h-cured 1.7 wt.% CNC sample demonstrated the lowest total weight loss (~ 9.6% lower than the control), indicating enhanced thermal resistance. Derivative weight analysis further confirmed this, showing the lowest peak weight change rate (0.105%/℃) for the 1.7 wt.% CNC sample cured for 48 h, compared to 0.304%/℃ for the unreinforced control. Additionally, differential scanning calorimetry (DSC) indicated reduced exothermic heat flow in 48-h-cured samples, especially in the 1.7 wt.% CNC formulation, suggesting minimal phase transitions and improved thermal reliability. The novelty of this work lies in demonstrating the synergistic enhancement of thermal resistance through CNC addition and extended curing. Unlike prior studies that primarily focused on mechanical reinforcement, this research establishes an optimal CNC dosage (1.7 wt%) that minimizes thermal degradation, offering critical insights for thermally stable, bio-reinforced geopolymer development. These findings support

Handling Editor: Mohammad Naraghi.

Address correspondence to E-mail: roopcr@unisa.ac.za

https://doi.org/10.1007/s10853-025-11638-3

the application of CNC–geopolymer composites in fire-resistant, sustainable construction materials.

GRAPHICAL ABSTRACT

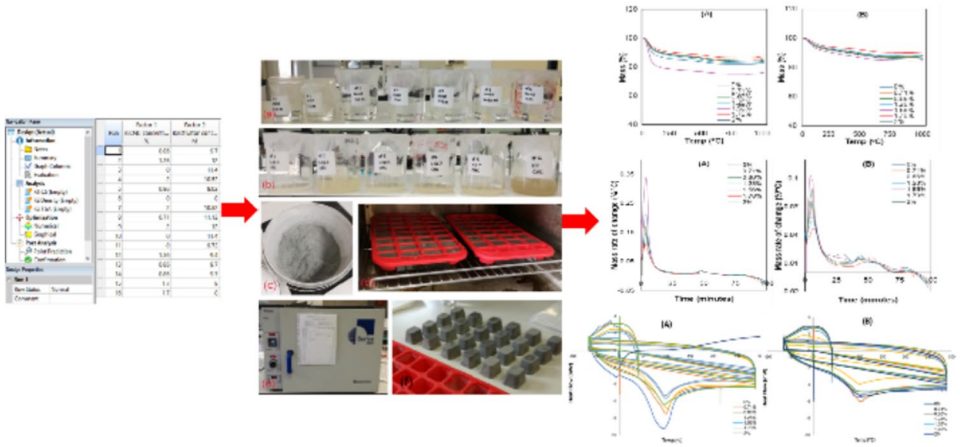

Introduction

The thermal stability of geopolymer construction materials is a critical attribute for infrastructure exposed to high temperatures, such as refractory linings, fire barriers, and kiln structures. Compared to Ordinary Portland Cement (OPC)—which typically emits ~ 1.0 tonne CO_2 per tonne produced and requires calcination above ~ 1400 ℃—fly ash-based geopolymer (FAG) shows much lower carbon footprints [1, 2]. A recent life-cycle assessment (LCA) study reports that low-calcium FAG can emit 14–28% less kg-CO_2eq than OPC concrete [3]. Another LCA study by Shi et al. [4] shows a reduction of up to ~ 62.7% CO_2 emissions under optimal activator and mixture design conditions. In terms of strength and high-temperature performance, mixtures incorporating FAG with binders can make it reach compressive strengths between 44 and 50 MPa, losing strength progressively when exposed to 300–700 ℃, but maintaining significant residual strength at elevated temperatures [5]. In fly ash-petroleum sludge ash geopolymer mortar, strength degradation becomes noticeable above 600 ℃, with matrix damage evident; decomposition of the geopolymer matrix begins near that temperature [6]. These recent findings show that FAGCs are capable of delivering mechanical strength comparable to OPC, while offering CO_2 reductions of ~ 20–60% and maintaining useful structural capacity under high-temperature exposure.

In efforts to enhance the performance of these eco-friendly binders, recent research has turned to nanomaterial reinforcement. Among these, cellulose nanocrystals (CNCs), which are renewable, bio-based additives derived from plant biomass, have attracted significant attention. CNCs have been found to improve mechanical properties such as compressive strength, fracture toughness, and resistance to microcracking when incorporated into cementitious or geopolymer matrices [7]. However, the majority of these investigations have focused on ambient or mechanical conditions, rarely extending into the thermal behavior domain. This leaves a substantial gap in our understanding of how CNCs influence thermal decomposition, weight-loss kinetics, or phase transformations in geopolymer composites.

Some existing studies involving other nanomaterials, such as nano-alumina, silica fume, and slag blends, have shown promising results in improving the durability and mechanical strength of geopolymers. Yet, few have assessed the implications of such additives under thermal stress. For example, Rovnaník and Šafránková [8] observed that fly ash geopolymers underwent strength gains up to approximately 800 ℃ due to crystallization phenomena, particularly the formation of albite above 900 ℃. Nevertheless, these systems still exhibited thermal deformation at elevated exposures. Likewise, Javed et al. [9] studied the thermal resilience of slag-blended and silica-modified geopolymer matrices

and reported encouraging strength retention, but they also documented noticeable microstructural shrinkage and weight loss during exposure to high temperatures ranging from 800 ℃ to 1200 ℃. These results point to the need for more holistic evaluations that go beyond mechanical metrics to include quantifiable thermal data.

Moreover, computational simulations have recently provided insights into the influence of chemical structure on thermal behavior. Molecular dynamics studies suggest that the silicon-to-aluminum (Si/Al) ratio and residual moisture content significantly affect thermal conductivity in geopolymers. A higher Si/Al ratio has been associated with increased heat transfer capabilities, while water molecules embedded in the matrix can disrupt phonon transport, influencing thermal resistance [10]. Although valuable, these studies remain theoretical and do not account for skeletal reinforcement or nano-additive effects such as those offered by CNCs.

An equally important consideration in thermal performance studies is the curing methodology. The curing process, which governs the final microstructure of geopolymer binders, varies significantly across the literature in terms of temperature, duration, and activator ratios. Such inconsistencies have made it difficult to establish universally effective curing protocols. Diab [11] demonstrated that steam curing helped reduce porosity and improve early mechanical strength by promoting aluminosilicate polymerization. However, contrasting results from a 2023 comparative study by Saludung et al. [12] on fly ash/slag systems indicated that while curing conditions influenced early-age strength, they had minimal impact on long-term thermal performance. These conflicting outcomes highlight the need for empirical frameworks that unify nanomaterial reinforcement strategies with optimized curing practices.

What is notably missing from the literature is a comprehensive, experimental investigation that evaluates how CNCs influence thermal degradation patterns in geopolymer composites, especially in tandem with various curing regimes. While CNCs have been employed to enhance moisture retention and mechanical behavior, their thermal decomposition characteristics and interactions with geopolymer matrices at elevated temperatures have not been rigorously studied. Additionally, no clear consensus exists regarding the optimal CNC concentration for balancing mechanical enhancement and thermal stability.

This study seeks to address these research gaps through an integrated thermal analysis of CNC-reinforced fly ash geopolymers. Using thermogravimetric analysis (TGA) and differential scanning calorimetry (DSC), the investigation focuses on quantifying mass-loss patterns, derivative weight behaviors, and heat-flow dynamics across a range of CNC concentrations. By comparing geopolymer samples cured for 24 h with those cured for 48 h, the study further explores how curing duration influences thermal resistance, particularly in relation to CNC content.

In bridging the gap between thermal analysis and sustainable material design, this work offers a novel contribution to the field of geopolymer science. Unlike previous efforts that either focused on mechanical behavior or employed nonrenewable nano-additives, this study integrates CNC-based reinforcement with rigorous thermal evaluation. It thereby introduces a new direction for enhancing the performance and sustainability of next-generation construction materials.

Literature review

The thermal performance of geopolymer materials has long been studied through techniques such as thermogravimetric analysis (TGA) and differential thermal analysis (DTA). TGA provides detailed information on weight loss across a temperature spectrum, while DTA captures temperature deviations between a sample and reference under uniform thermal regimes. In more recent research, differential scanning calorimetry (DSC) has also been deployed to quantify heat-flow transitions within geopolymer matrices [13]. Together, TGA, DTA, and DSC form a triad of analytical tools that illuminate dehydration, dehydroxylation, phase transitions, and sintering phenomena in geopolymer systems, offering insights that underlie both performance and durability.

The earliest foundational work by Rickard and van Riessen [14] still offers valuable benchmarks for fly ash-based geopolymer (FAG) thermal behavior. Their TGA results demonstrated up to 80% of total mass loss below 200 ℃, attributed to free and loosely bound water loss, followed by gradual mass loss between 200 and 400 ℃ due to chemically bound water. A prominent exothermic peak at approximately 418 ℃ captured the transformation of ferrihydrite into hematite. Intriguingly, above 600 ℃, a net weight gain emerged as oxidized iron species within the matrix reacted,

particularly in cracked regions exposing Fe phases to atmospheric oxygen. Their DTA curve confirmed continued dehydration up to 250 ℃ and showcased exothermic reactions coinciding with weight changes [14]. Although this work was published more than a decade ago, it remains a cornerstone reference for thermal event mapping in FAGs.

Further refinement in temperature-event mapping was achieved by Rosas-Casarez et al.[15], who established a clear demarcation of weight-loss zones: about 10% mass lost between 0 and 120 ℃ (surface water evaporation), another 10–15% between 120 and 200 ℃ (release of geopolymeric gel water), and additional loss between 450 and 800 ℃ associated with carbonate decomposition. This work provided a segmented view of the thermogram and served as a robust reference for understanding dehydration, dehydroxylation, and decarbonation in aluminosilicate matrices [15].

Caballero et al. [16] extended the application of TGA–DTA methods to metakaolin geopolymer samples under inert conditions (up to 1000 ℃ at 10 ℃/min). They reported a 10–15% mass loss below 300 ℃ due to free water evaporation, followed by approximately 2% loss between 350 and 700 ℃, attributed to the removal of hydroxyl groups during dehydroxylation. Notably, weight loss beyond 600 ℃ was minimal (< 0.3%), suggesting negligible decomposition at high temperature under inert atmospheres. Despite focusing on metakaolin rather than fly ash, this study provided a comparative perspective on precursor-dependent thermal behavior [16].

Lemougna et al. [17] further analyzed metakaolin-based composites reinforced with quartz–feldspar sand or glass wool, subjecting samples to TGA up to 1200 ℃. These composites retained 93–96% of their mass even at 1200 ℃. Mass-loss profiling indicated hygroscopic water evaporation below 100 ℃, loss of structurally bound water between 100 and 300 ℃, and condensation reactions among Si–OH/Al–OH groups between 300 and 800 ℃. Beyond 800 ℃, sintering dominated over decomposition, marking the onset of ceramic-phase formation. The high thermal retention values reported (93–96%) underscored the potential of aggregate reinforcement for high-temperature geopolymer stability [17].

He et al. [18] offered a comprehensive comparison between metakaolin, fly ash, and boiler slag blends. Their TGA and DTA analyses identified minor endothermic peaks (50–150 ℃) due to evaporation of adsorbed water, and larger exothermic peaks (300–500 ℃) associated with mineral transitions. Importantly, whereas metakaolin geopolymer lost nearly 13% by 600 ℃, slag-modified blends lost only about 9.4% by 1250 ℃, highlighting how precursor chemistry and slag admixture influence thermal stability. This study also contrasted values against traditional cement pastes, which showed ~ 25% weight loss by 600 ℃. These quantitative differences illuminate the influence of industrial waste admixtures and underscore the necessity of TGA–DTA profiling for benchmarking geopolymer resilience.

In more recent literature, the thermal stability of FAG paste, mortar, and lightweight concrete has been quantified using combined TGA–DSC approaches. Zhao, et al. [19] studied high-volume FAG mixtures cured at ambient temperature and exposed to elevated temperatures. Their results demonstrated that the residual compressive strength retained a significant fraction even after exposure to 800 ℃. TGA indicated a mass loss of approximately 15–20% below 300 ℃, followed by slower degradation up to 800 ℃. DSC peaks corroborated energy-intensive transitions around 350–450 ℃. When compared with OPC-based systems, the FAG exhibited stronger residual mechanical performance post-thermal exposure, further validated using XRD and SEM imaging [19].

More recently, thermal stability has been examined in lithium slag–FAG exposed to 900 ℃ (2023–24). That study reported mass losses ranging from 12 to 18% at 900 ℃, depending on silica-fume content, and documented higher crystalline phase evolution at higher exposures. The inclusion of silica fume modulated mass-loss behavior by limiting shrinkage and stabilizing geopolymer gels [20]. These findings quantified how key parameter changes, including precursor composition, affect thermal performance.

In parallel, Sicilian clay-based geopolymer systems have been studied through TGA and DSC combined with principal component analysis (PCA) to statistically link preparation conditions to thermal behavior outcomes. One such investigation revealed that geopolymer samples with higher metakaolin content showed higher mass loss (~ 15% by 600 ℃) compared to hybrids with other additives (~ 10%). DSC curves identified dehydration peaks near 100 ℃ and sintering-associated exothermic transitions near 600–900 ℃. Statistical clustering further demonstrated strong correlations between NaOH concentration, Si/Al ratio, and onset degradation temperature [21].

Another recent study of ultra-high-performance geopolymer composites (UHPGCs) reinforced with cellulose nanofibers (CNFs) demonstrated that CNF content at 1% by weight improved thermal resistance—mass loss at 600 ℃ was only about 8%, compared with 11–12% for control samples without reinforcement. DSC corroborated lower enthalpy changes in the CNF composites, suggesting reduced thermal reactivity [22]. This progress indicates that bio-based cellulose reinforcements, such as nanofibers or nanocrystals, can meaningfully influence thermal resilience.

Though these recent papers highlight thermal trends, explicit investigations of cellulose nanocrystal (CNC) reinforcement on geopolymer thermal behavior remain scarce. CNCs possess good inherent thermal stability (T_{50} degradation between 300 and 350 ℃) according to thermogravimetric data (TGA) on CNC suspensions [23–25], suggesting that their incorporation into geopolymers may alter thermal degradation pathways. Elsewhere, CNC addition has been shown to enhance bonding within cementitious matrices and modulate setting characteristics, offering promise for thermal applications [26]. Yet there remains no quantified report on CNC dosage impacts on TGA mass-loss profiles, derivative weight behavior, or onset temperature changes in geopolymer materials.

Similarly, atomistic simulations exploring thermal conductivity in carbon nanotube-reinforced geopolymers concluded that high nanoreinforcement content (e.g., 16.5 wt%) can significantly increase thermal conductivity (from 2.15 to 4.85 W/m·K), although phonon scattering at interfaces remains a limiting factor [27]. While not directly about CNCs, these studies underscore the importance of nanoscale enhancement on thermal transport, but leave unknown their influence on weight-loss kinetics or phase stability.

Furthermore, molecular dynamics simulations examining Si/Al ratio and moisture content link thermal conductivity trends to structural parameters were conducted by Liu & Ju [20]. The authors showed that moisture level and aluminosilicate composition alter heat transport: a 5% moisture content resulted in ~ 40% reduction in thermal conductivity when compared to dry counterparts [20]. Although useful, these simulation insights do not incorporate experimental validation, especially under variation in CNC reinforcement or curing strategy.

One important challenge across studies is inconsistency in curing procedures, which significantly affects both mechanical and thermal outcomes. Diab [11] reported that steam curing at 60 ℃ for 24 h yielded superior geopolymer network formation, reduced microporosity, and enhanced early-age strength when compared to ambient curing. However, a later study by Saludung et al. [12] observed that the curing protocol had limited influence on performance when exposed to 800–900 ℃, suggesting that the curing–thermal performance link may be complex and dependent on additive chemistry. Another study by Tran et al. [28] using graphene nanoplatelet reinforcement emphasized that curing duration interacts with nano-additive dispersion, affecting heat resistance up to 400–600 ℃; however, extending these findings to CNC–geopolymer interactions remains unexplored.

In summary, published studies effectively demonstrate how precursor materials (fly ash, metakaolin, slag), curing strategies, and reinforcement additives influence thermal behavior. Quantitative thermal values are available in many cases: weight losses near 10–15% by 300 ℃, mass retention of ~ 93–96% at 1200 ℃ in aggregate composites, and ~ 12–18% mass loss at 900 ℃ in lithium slag systems, among others. Dehydration and dehydroxylation events dominate below 400–500 ℃, while sintering or ceramic-phase formation may take precedence beyond 800 ℃, depending on composition. Despite this, research gaps remain: the effect of bio-based CNC reinforcement on thermal stability is virtually uninvestigated, particularly in FAGs; systematic exploration of CNC dosage and curing interactions is absent; and few studies combine TGA, DSC, derivative analysis, and phase mapping in one robust analytical framework. The analyses from the reviewed research were consolidated (Table 1) to form a baseline to interpret thermal analyses in future studies (and this study).

By filling these gaps, our study endeavors to connect CNC dosage (0–1.86 wt%), curing duration (24 vs. 48 h), and thermal behavior via TGA and DSC investigations. We focus on derivative mass-loss kinetics, onset degradation temperature shifts, and heat-flow transitions. Preliminary observations point to CNC concentrations around 1.7 wt% as optimal for reducing total mass loss and smoothing derivative peaks, while extended curing time enhances matrix encapsulation and thermal resilience. These findings aim to unify

Table 1 Literature thermal analyses

Author (Ref)	Temperature	Observation	Explanation
Rickard and van Riessen [14]	< 80 ℃	The DTA plot shows an endothermic peak	Dehydration of loosely bound and adsorbed water
Lemougna et al. [17]	< 100 ℃	Weight loss	Hygroscopic water evaporation
Rosas-Casarez et al. [15]	< 120 ℃	The first decline in the TGA curve	Evaporation of moisture from the sample's surface and pores
He et al. [29]	50–150 ℃	Endothermic peak in the TGA plot	Free water evaporation
Rickard and van Riessen [14]	< 200 ℃	80% of the total weight loss	Geopolymer dehydration
Rosas-Casarez et al. [15]	120–200 ℃	Thermal degradation in the TGA curve	Sodium aluminum silicate hydrate formation
Rickard and van Riessen [14]	80–250 ℃	Endothermic trace	Further dehydration of the geopolymer sample
Caballero et al. [16]	22–300 ℃	Two endothermic peaks in the DSC curve correspond to a 10–15% weight loss	Humidity reincorporation resulting from the loss of free or loosely bound water
Lemougna et al. [17]	100–300 ℃	Weight loss	Evaporation of structural moisture from the geopolymer matrix
Rickard and van Riessen [14]	200–400 ℃	Mild weight loss	Gradual dehydration of chemically bound residual water
He et al. [29]	300–500 ℃	Exothermic peak	Phase transformation of mineral constituents
Caballero et al. [16]	350–700 ℃	2% weight loss	Dehydroxylation of the geopolymer framework Moisture release facilitates the formation of Si–O–Si bonds
Lemougna et al. [17]	300–800 ℃	1–2% weight loss	Elimination of structural water is accompanied by the condensation of Si–OH and Al–OH groups within the geopolymer gel Si–O–Si group and Si–O–Al group formation
Rickard and van Riessen [14]	418 ℃	Large exotherm	Transformation of ferrihydrite into hematite
Rickard and van Riessen [14]	400–600 ℃	Weight loss	Dehydroxylation of ferrihydrite during its crystallization into hematite
Rosas-Casarez et al. [15]	450–800 ℃	Third thermal degradation	Weight loss in the carbonates range
Caballero et al. [16]	600 ℃	< 0.3% weight loss	Further water release
He et al. [29]		13% weight loss	
Rickard and van Riessen [14]	> 600 ℃	Weight gain	Elevated temperature exposure leads to the viscous flow of aluminosilicate phases, potentially causing microstructural cracking Oxidation of Fe species occurs upon exposure to atmospheric oxygen
Lemougna et al. [17]	> 800 ℃	No significant weight loss	Thermal decomposition reactions are largely complete beyond this point Initiation of sintering processes at high temperatures Formation of the ceramic body

previous literature's strengths—quantitative thermal data, parameter effect analysis—with new insights on sustainable biochemical nanoreinforcement, producing actionable guidelines for designing heat-resistant, green geopolymers.

Materials and methods

Materials

The fly ash was obtained from the Eskom Matla Power Station in South Africa. It was selected as an appropriate precursor due to its classification as Class F fly ash, a Si/Al ratio of approximately 1, and its low organic content, indicated by a loss on ignition (LOI) value of < 5%. Sawdust was sourced from Sappi sawmills, also located in South Africa. The CNC produced through proprietary technology was incorporated as a reinforcing additive in the synthesis of the geopolymer [7].

Geopolymer mixture design

A trial-and-error approach was employed to optimize the proportions of fly ash, water, alkaline activator, and CNC suspension. The best-performing mix consisted of 60.8 mL of the combined liquid phase (alkaline activator plus CNC suspension) per 100 g of fly ash, yielding a workable consistency suitable for molding. The liquid phase itself was formulated as a 25% CNC suspension and 75% alkaline activator [7].

Statistical experimental design

The concentrations of both the alkaline activator solution and the CNC suspension were systematically varied across the trials. Statistical design of experiments (DoE) was conducted using Design Expert software to streamline the number of required runs. After defining the optimization objective, a response surface methodology (RSM) was selected, allowing the combined influence of activator and CNC concentrations to be visualized as a single 3D surface. Based on the specified design criteria, the software generated the experimental matrix—comprising 16 experimental runs—which is presented in Table 2 [7].

Table 2 The generated experimental runs from Design Expert [7]

Run	Factor 1 A: CNC concentration (%)	Factor 2 B: activator concentration (M)
1	0.86	9.7
2	1.28	12
3	0	11.4
4	2	10.52
5	0.86	8.02
6	0	8
7	2	10.52
8	0.71	11.12
9	2	12
10	0	11.4
11	0	9.72
12	1.56	9.4
13	0.86	9.7
14	0.86	9.7
15	1.7	8
16	1.7	8

Geopolymer synthesis

Preparation of solutions

Freeze-dried CNC was incorporated into the predetermined volumes of deionized water to achieve the target solution concentrations [1] (see Table 2). These mixtures were agitated continuously overnight to ensure full hydration and uniform dispersion. The range of CNC concentrations followed values recommended in the literature [30–32]. Concurrently, sodium hydroxide (NaOH) pellets were accurately weighed and dissolved to produce activator solutions at the specified concentrations detailed in Fig. 1.

Geopolymer molding

For each trial defined by the design matrix (see Fig. 1), 100 g of fly ash was placed in a glass beaker and combined with the prescribed volumes of alkaline activator and CNC solutions. The mixture was stirred until a smooth, homogeneous paste was obtained, then cast into silicone molds [7].

Geopolymer curing

The silicone-molded geopolymer pastes were placed in an oven preheated to 40 ℃, and two distinct curing protocols were assessed [7]:

Protocol A:

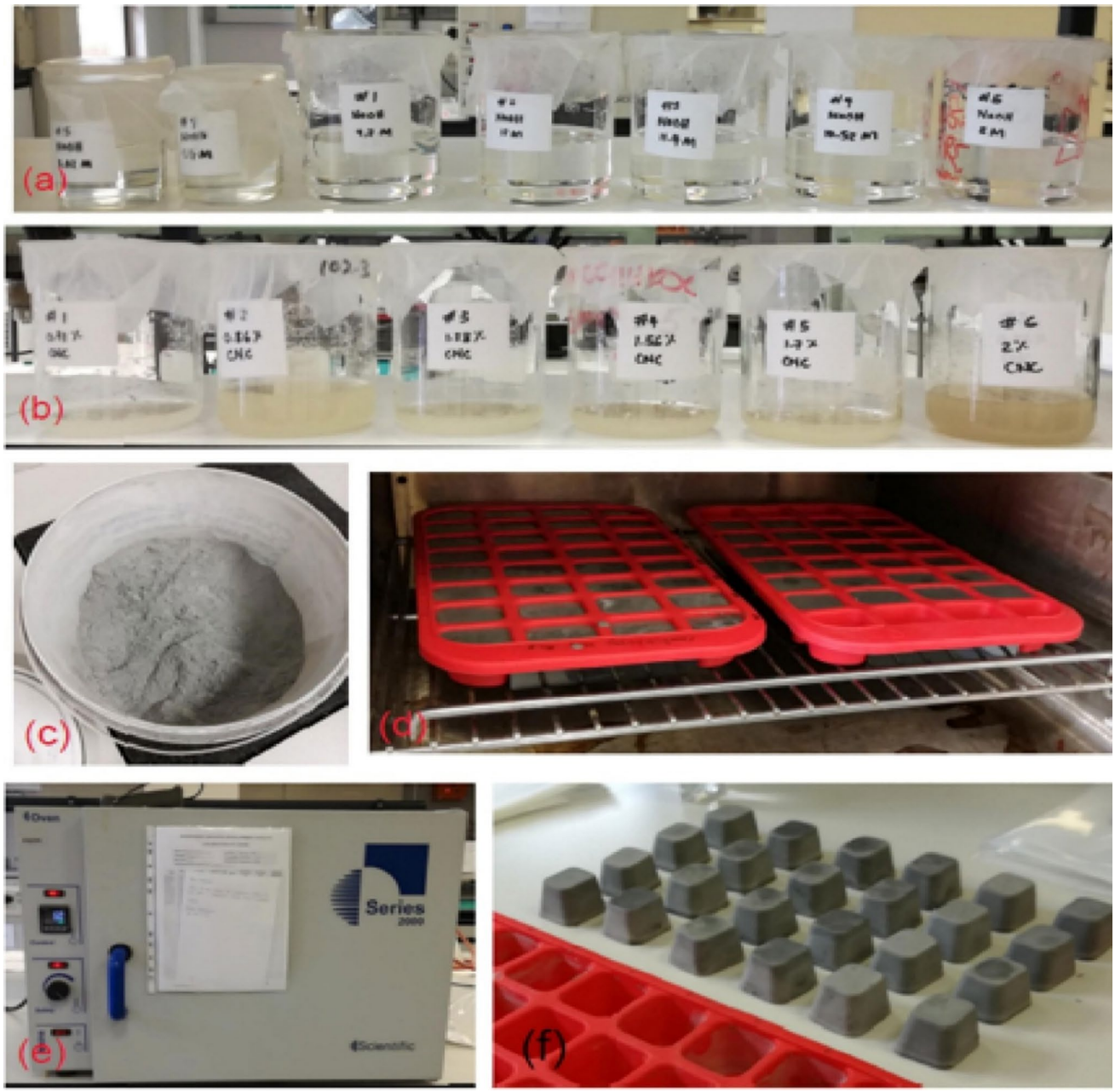

Figure 1 **a** Alkaline activator solutions **b** CNC solutions **c** Fly ash **d** Molded geopolymer pastes prior to curing **e** Oven used for curing (f) De-molded geopolymers post-curing [7].

Hold at 40 ℃ for 2 h
Increase to 60 ℃ for 24 h
Rotate the samples, then continue curing at 60 ℃ for an additional 24 h to ensure even heat distribution

Protocol B:

Hold at 40 ℃ for 2 h

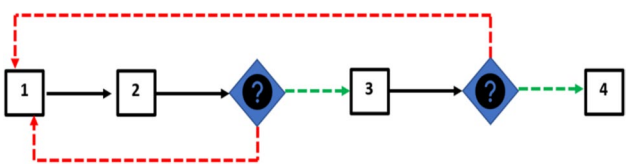

Figure 2 Graphical depiction of the iterative empirical curing framework.

Increase to 60 ℃ for 24 h
No rotation or further curing

The entire synthesis sequence is detailed in Steps 1–4 and depicted in Fig. 2. From these iterative trials, an optimized curing framework has been developed. These protocols were also repeated for a 48-h duration. It should be noted that the maximum time investigated in this study was 48 h.

Step 1 (Evaporation)

The first two hours of curing are regarded as the "evaporation phase"—when moisture rapidly evaporates from the sample. The evaporation phase must be cured at a relatively low temperature (not exceeding 40 ℃) to prevent cracking.

Step 2 (Phase 1)

2.1 Choose the curing duration. If oven curing is used, then 24 h and multiples thereof are required. Microwave curing can also be used and has been found to work more effectively than oven curing [33, 34]. If oven curing is used, cure for 24 h.

2.2 Choose the curing temperature: after the evaporation phase, the phase 1 temperature can be increased by up to 20 ℃. A greater temperature increase is not advised, as rapid temperature differentials lead to rapid moisture evaporation from the sample pores, thus leading to cracking.

2.3 If surface cracking is observed after phase 1, lower the evaporation phase temperature and restart the process.

2.4 If no surface cracking is observed, proceed to the de-molding phase.

Step 3 (De-molding)

3.1 Using thermal gloves, carefully remove the sample molds from the oven, lay them on a flat surface, and remove the samples from the mold. Once removed, turn the samples over and place them over the molds.

Step 4 (Phase 2)

4.1 Place the rotated samples back into the oven at the same temperature and duration as phase 1.

4.2 If any cracking is observed after phase 2, restart the process, but lower the phase 2 temperature.

4.3 If no cracking is observed, then the curing process is complete.

Geopolymer testing

Geopolymer samples were analyzed using a combined TGA/DSC system (Model Q500/Q2000, TA Instruments, USA) under a controlled temperature program. Each sample was heated at 2.08 ℃ min^{-1} from room temperature to 290 ℃ for DSC measurements and to 1,000 ℃ for TGA measurements, while purged with nitrogen at 25 mL min^{-1}. This configuration enabled simultaneous recording of weight loss (TGA) and DSC [35]. The TGA data quantified sample weight change as a function of temperature, and the DSC traces were used to pinpoint endothermic and exothermic events unrelated to weight variation. The weight change of each sample was recorded continuously as temperature increased [35]. In parallel, DSC measurements were performed to resolve endothermic and exothermic transitions associated with thermal events that occur without accompanying weight loss.

Results and discussion

Thermogravimetric analysis

General trends

As mentioned earlier, two curing times were investigated in this study for the samples, and the TGA results are illustrated in Fig. 3. Generally, most of the 24-h-cured samples (with the exception of the 0.86 wt.% CNC dosage) exhibited a steep weight loss just before reaching 100 ℃ (see Fig. 3A). This weight loss could be attributed to the following reasons: de-watering as free and adsorbed moisture evaporated from the sample [16], dehydration of adsorbed and loosely bound water [14], humidity reincorporation [16], and the evaporation of hygroscopic water [17]. Afterward, a gradual weight loss was observed between 100 ℃ and 600 ℃ until the weight remained constant between 600 ℃ and 950 ℃. The gradual weight loss was attributed to hydroxyl group (-OH) elimination, forming silicon–oxygen–silicon bonds, eliminating structural water [16, 17], and the dehydroxylation of ferrihydrite [14].

The 48-h-cured samples (Fig. 3B) displayed a thermal behavior similar to that of the 24-h-cured counterparts. A sharp weight loss was observed as the temperature rose to 100 ℃, primarily due to rapid moisture evaporation. Beyond 100 ℃, a more gradual reduction in weight was noted, likely resulting from the progressive thermal degradation of CNC within the matrix. This assumption is supported by the literature, indicating that CNC begins to degrade between 150 ℃

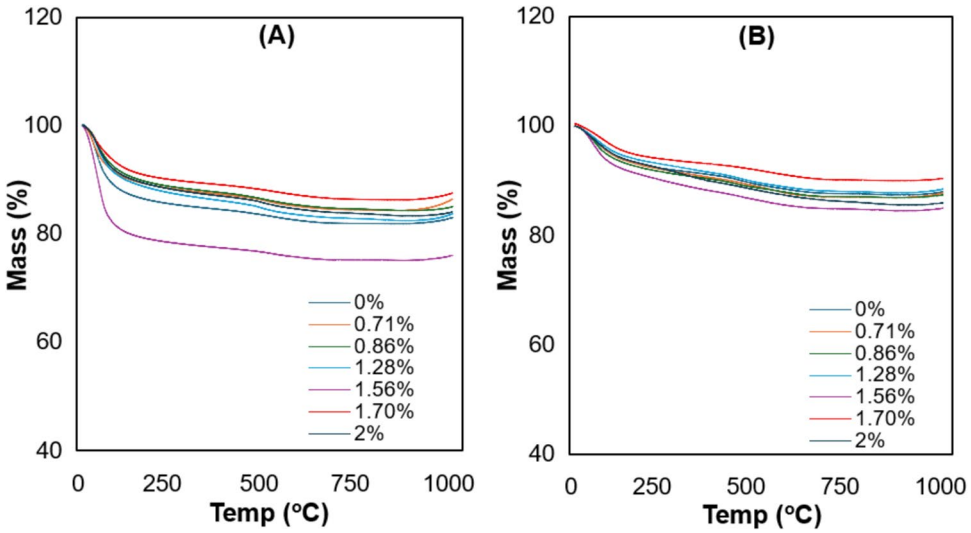

Figure 3 TGA curves of **A** 24-h-cured samples **B** 48-h-cured samples.

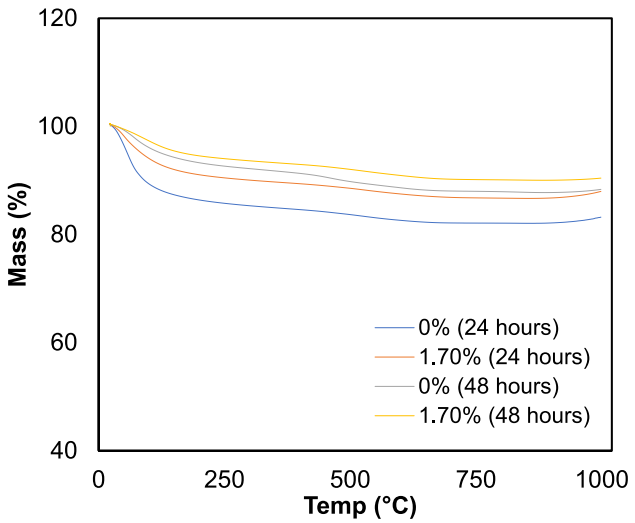

Figure 4 Weight-loss behavior of the control and optimal CNC-dosed sample.

and 200 ℃ [36]. Additionally, the sample preparation method—involving pulverization prior to thermal analysis—facilitated more efficient CNC decomposition under elevated temperatures compared to intact solid samples.

Comparative thermogravimetric analyses

The TGA curves (Fig. 4) indicate that the initial weight losses of the 24-h and 48-h-cured control samples were similar. However, the 24-h-cured samples exhibited a steeper weight loss as the temperature rose to 100 ℃. While both sets of samples continued to lose weight gradually after reaching 100 ℃, the 24-h-cured samples experienced greater weight loss compared to the 48-h-cured ones. This higher weight loss in the 24-h-cured samples could be attributed to two potential factors: first, incomplete combustion of the organic components in the geopolymer precursors. This finding was confirmed by the precursor fly ash's organic content not exceeding 5%. Second, the shorter curing duration led to incomplete stabilization of the organic constituents within the geopolymer matrix. As a result, these residual organics remained vulnerable to thermal shrinkage and combustion during high-temperature exposure, contributing to a greater overall weight loss in the sample. Although the CNC-dosed samples did not begin with identical initial weights, the 24-h-cured samples consistently exhibited greater weight loss than those cured for 48 h, likely due to incomplete network formation and residual moisture retention in the shorter curing duration. Interestingly, no linear correlation was observed between CNC concentration and thermal weight loss across the samples. This nonlinearity can be attributed to the dual role CNCs play in geopolymeric matrices. At lower dosages, CNCs act as nano-fillers in geopolymer matrices: they enhance matrix densification and thermal resistance via hydrogen bonding with aluminosilicate gel phases and improved interfacial adhesion, which can limit mass loss during thermal decomposition [31]. Conversely, at higher CNC concentrations, researchers observed agglomeration and reduced composite homogeneity, leading to weaker zones that can initiate thermal degradation under heat exposure [37, 38].

The observed minimum weight loss at 1.7 wt.% CNC suggests an optimal balance between reinforcement dispersion and matrix integrity, beyond which additional CNCs may impair thermal performance due to poor dispersion and limited matrix encapsulation. Moreover, under increasing temperature conditions, the 1.7wt.% CNC formulation showed the most gradual and minimal weight reduction, further reinforcing its effectiveness in improving thermal stability.

Optimal doped vs baseline concentration comparison

The total average weight losses for the baseline sample (0% CNC) and those with varying CNC concentrations were calculated and are presented in Fig. 5. It was observed that samples cured for 48 h consistently exhibited lower weight loss across all CNC dosages compared to those cured for 24 h. Among the tested concentrations, the 1.7% CNC dosage resulted in the least weight loss under both curing conditions, indicating enhanced thermal resistance. Consequently, 1.7wt. % CNC was identified as the optimal concentration for minimizing thermal degradation. Combining the 1.7 wt.% CNC dosage and the 48-h curing condition is recommended to minimize the sample weight loss. This finding is shown in Fig. 5, which compares the weight loss of the baseline sample to that of the optimal 1.7wt.% CNC dosage under both curing conditions.

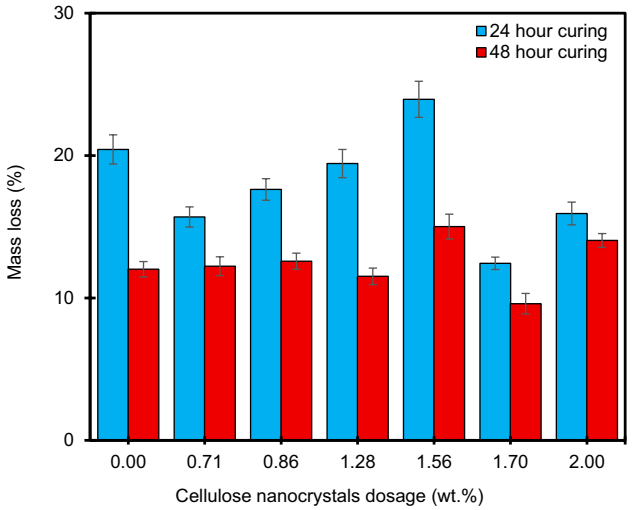

Figure 5 Overall average weight loss at each dosage of CNC.

Derivative weight plots

The derivative weight plots illustrated the rate at which the sample weight changed over time. For all 24-h-cured samples, the general trend featured an initial dip, followed by two distinct peaks, as shown in Fig. 6A. The first peak appeared around the 5-min mark, while the second occurred approximately at 48 min. The first peak was characterized by sharp increases and decreases, indicating a period of rapid weight change. This suggests that the most significant loss occurred within the first 5 min of the analysis. Beyond this point, the rate of weight loss stabilized momentarily before experiencing a sharp decline between 5 and 10 min. Following the initial rapid changes, the derivative weight values gradually

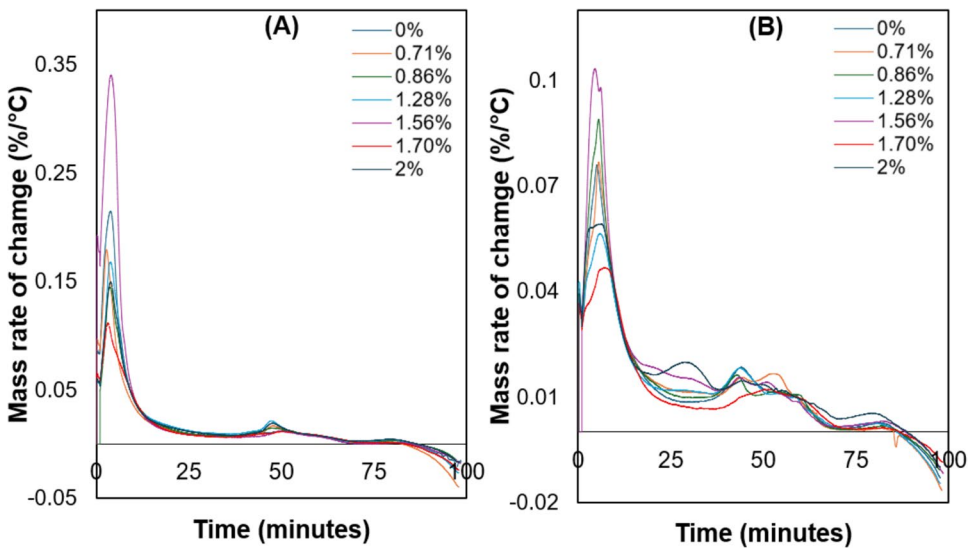

Figure 6 Derivative weight change for **A** 24-h-cured samples and **B** 48-h-cured samples.

declined between 10 and 30 min, then remained relatively stable from 30 to 42 min. Around the 48-min mark, all samples exhibited a notable rise and subsequent fall in derivative weight, forming their respective second peaks. These second peaks reflected minor changes, with derivative weight rates below 0.05%/℃.

Among the samples, the 1.56% CNC dosage displayed the most pronounced first peak at approximately 0.34%/℃, indicating a rapid initial weight loss. This was followed by the 0 wt.% CNC sample, which reached around 0.22%/℃. The remaining CNC-dosed samples exhibited lower first peak values, all under 0.2%/℃. Given that the 1.56 wt.% CNC formulation also showed the greatest overall weight loss and the poorest thermal stability in the TGA analysis; the high derivative peak further supports its classification as thermally less stable.

Aside from the 1.56 wt.% CNC dosage, the 0% CNC sample exhibited the highest peak among the other CNC concentrations. This peak represented the sharpest rate of weight change with increase in temperature, suggesting that incorporating CNC enhances the thermal stability of the geopolymer matrix. Notably, the 1.7 wt.% CNC dosage demonstrated only a subtle peak, reinforcing its classification as the most thermally stable formulation, consistent with previous weight-loss analyses, where this dosage showed the lowest weight reduction. As the analysis progressed beyond 85 min, the derivative weight values became negative, indicating a net gain in weight. This increase can be attributed to the oxidation of iron species at temperatures exceeding 600 ℃ [14]. Additionally, sintering reactions occurring above 800 ℃ may have contributed to the formation of a ceramic phase, resulting in a denser structure and corresponding weight gain [17].

The derivative weight change values for the 48-h-cured geopolymer samples were generally lower than those observed for the 24-h-cured samples, with the highest recorded rate being 0.105%/℃ for the former, compared to 0.304%/℃ for the latter (see Fig. 6B). This notable difference highlights that the extended 48-h curing process enhanced the thermal and mechanical properties of the geopolymers. A consistent pattern was observed across all samples, showing pronounced peaks at around 5 min into the analysis, indicating that the most rapid fluctuations in sample weight occurred early during heating. Among the samples, the 1.56 wt.% CNC dosage had the highest peak, reaffirming its poor performance in terms of thermal stability. Conversely, the 1.7 wt.% CNC dosage displayed the lowest peak, aligning with earlier findings that identified it as the most thermally stable formulation.

Unlike the 24-h-cured samples, which typically exhibited two sharp peaks, the 48-h-cured samples demonstrated multiple, broader peaks throughout the test duration. Notably, all samples—regardless of curing time—showed a shift to negative weight change values just before the 90-min mark, likely due to oxidation and sintering effects at elevated temperatures. The transition in scale was attributed to the weight gain observed in the samples, as previously mentioned. The peaks for each CNC concentration were notably lower in the 48-h-cured samples compared to the 24-h-cured ones. This suggests that the samples experienced less weight loss when cured for 48 h compared to the 24-h curing duration.

Differential scanning calorimetry

The heat flow through a material indicates its thermal conductivity. For thermal resistance, low heat-flow capabilities are beneficial. The opposite holds for applications that require thermal conductivity. According to conventional heat transfer principles, a positive heat flow denotes heat absorption by the material, while a negative heat flow indicates the release of heat [7]. The 24-h-cured samples (Fig. 7A) exhibited an exothermic peak around 100 ℃, attributed to mineral phase transitions [29]. Positive heat-flow areas, on the other hand, reflected moisture reabsorption due to the evaporation of free water within the samples [16, 18]. The observed heat-flow values ranged from − 9.3 to 3.5 mW. At temperatures below 50 ℃, endothermic activity dominated, suggesting a higher prevalence of phenomena such as melting, sublimation, solid-state transitions, and certain chemical reactions [35]. The 48-h-cured samples (Fig. 7B) showed similar heat-flow behavior but within a narrower range (-6.02 to 2.9 mW), particularly on the exothermic side. This reduced range suggests that extended curing time suppressed heat flow from the material. Compared to the 24-h samples, the 48-h-cured samples displayed more consistent heat-flow patterns across all CNC concentrations. Notably, the 1.7 wt.% CNC dosage consistently exhibited the lowest exothermic peaks under both curing conditions (see Fig. 8), reinforcing previous conclusions from TGA and derivative weight change studies regarding its superior thermal stability.

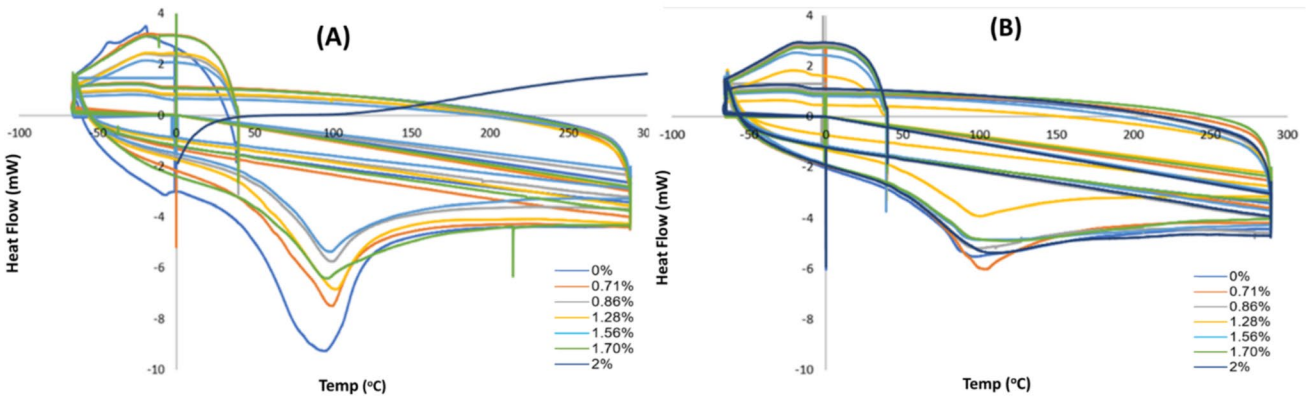

Figure 7 Heat-flow analysis for **A** 24-h-cured samples and **B** 48-h-cured samples.

Figure 8 Heat-flow comparison between the baseline and optimal CNC dosage with curing conditions influence.

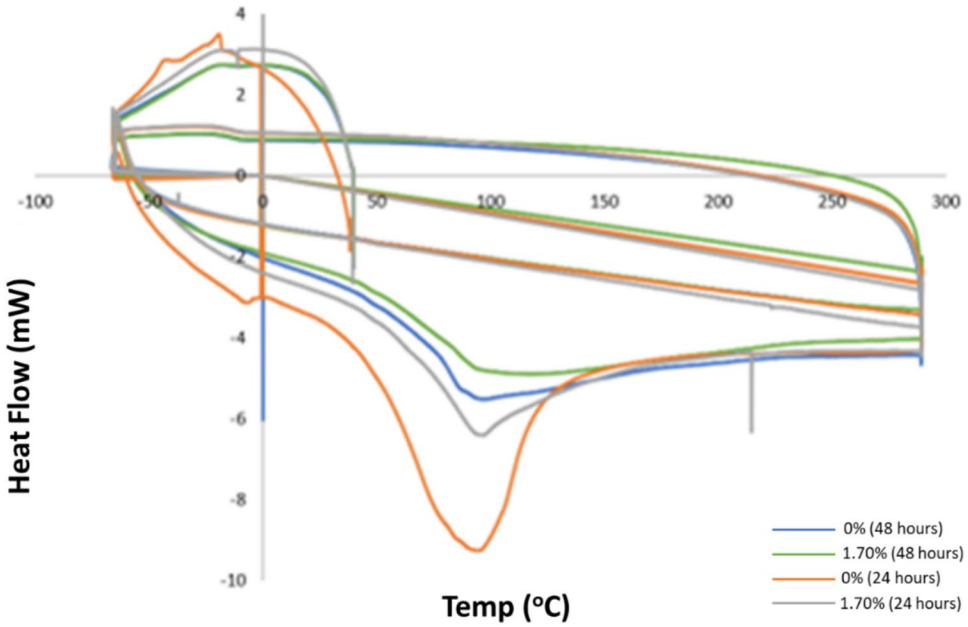

Conclusions

This study explored the thermal stability of fly ash-based geopolymers (FAG) modified with cellulose nanocrystals (CNCs), focusing on the influence of curing duration (24 and 48 h) and CNC content (ranging from 0 wt.% to 2.0 wt.%). Through thermogravimetric analysis (TGA), derivative thermogravimetry (DTG), and differential scanning calorimetry (DSC), several important insights were drawn about the material's thermal behavior.

Across all formulations, an initial rapid weight loss occurred below 100 ℃, primarily due to free moisture evaporation. This was followed by gradual mass loss up to around 600 °C, corresponding to dehydroxylation and the release of bound water. Samples cured for 48 h consistently showed lower total weight loss than those cured for 24 h, suggesting improved matrix consolidation and thermal resistance with extended curing. Notably, the geopolymer containing 1.7 wt.% CNC displayed the best performance, recording the lowest mass loss at 9.6% after 48 h of curing, compared to 11.7% for the control sample without CNCs.

Interestingly, the relationship between CNC content and weight loss was found to be nonlinear. At lower CNC dosages (around 1.28 wt.% or less), the nanoparticles appeared to enhance thermal resistance by improving matrix densification and establishing strong

hydrogen bonding within the geopolymer network. However, higher CNC contents (2.0 wt.% and above) led to agglomeration and network disruption, introducing weak spots that facilitated thermal degradation. The data pointed clearly to 1.7 wt.% CNC are the optimal reinforcement level, effectively balancing dispersion and structural integrity.

Further insights from DTG revealed distinct decomposition stages, particularly in 24-h-cured samples, where two significant weight-loss peaks were observed. The 1.56 wt.% CNC sample had the most intense degradation rate at 0.34%/°C, indicating lower thermal stability. In contrast, the 1.7 wt.% CNC formulation exhibited the slowest rate (≤ 0.12%/°C), reinforcing its superior thermal performance. This trend was further strengthened in the 48-h-cured samples, where all peak intensities were lower overall, with a maximum of just 0.105%/°C.

DSC analysis supported these observations. The 24-h-cured samples showed broader and more variable thermal activity, while the 48-h-cured samples demonstrated narrower, more stable heat-flow ranges. Again, the 1.7 wt.% CNC formulation exhibited the lowest exothermic peaks under both curing regimes, further validating its improved thermal insulation behavior.

Both curing duration and CNC dosage play a synergistic role in determining the thermal performance of geopolymer composites. The combination of 1.7 wt.% CNC with 48 h of curing yielded the most thermally stable system, offering valuable guidance for developing geopolymer materials for thermal insulation and structural applications. While this study provided valuable insights into the thermal stability of CNC-modified fly ash geopolymers, it did not examine parameters such as long-term durability, fire exposure cycles, or performance under varying humidity and environmental conditions. Future research should consider the effects of alternative nanomaterials, dynamic thermal loading, and real-world exposure scenarios. Additionally, large-scale fabrication techniques, life-cycle assessments, and cost-effectiveness analyses will be essential to bridge laboratory findings with practical applications in sustainable, heat-resistant construction and refractory materials.

Authors' contributions

R. Roopchund was involved in conceptualization, methodology, software, investigation, formal analysis, visualization, writing—original draft. L. Fajimi helped in visualization, writing—final draft. N. Seedat contributed to validation, writing—reviewing & editing. J. Andrew was involved in conceptualization, validation, supervision, writing—reviewing & editing.

Funding

This research was supported by the South African Department of Science and Innovation (DSI)—Council for Scientific and Industrial Research (CSIR) Biorefinery Research Consortium under Contract Number 0188/2017.

Declarations

Competing interests The authors declare that they have no competing personal relationships or financial interests.

References

[1] Zhuang XY et al (2016) Fly ash-based geopolymer: clean production, properties and applications. J Clean Prod 125:253–267. https://doi.org/10.1016/j.jclepro.2016.03.019

[2] Huntzinger DN, Eatmon TD (2009) A life-cycle assessment of Portland cement manufacturing: comparing the traditional process with alternative technologies. J Clean Prod 17(7):668–675. https://doi.org/10.1016/j.jclepro.2008.04.007

[3] Singh GVPB, Prasad VD (2024) Evaluating the performance and environmental impact of low calcium fly ash-based geopolymer in comparison to OPC-based concrete. Environ Sci Pollut Res 31(59):66892–66910. https://doi.org/10.1007/s11356-024-35715-3

[4] Shi X et al (2021) Life cycle assessment and impact correlation analysis of fly ash geopolymer concrete. Materials. https://doi.org/10.3390/ma14237375

[5] Pratap B, Kumar P (2023) Effect of the elevated temperature on the mechanical properties of geopolymer concrete using fly ash and ground granulated blast slag. J Struct Fire Eng 15(3):409–425. https://doi.org/10.1108/JSFE-06-2023-0028

[6] Usman Kankia M, Baloo L, Danlami N, Zawawi NA, Bello A, Muhammad SI (2023) Microstructural analysis and compressive strength of fly ash and petroleum sludge ash geopolymer mortar under high temperatures. Sustainability 15(12):9846. https://doi.org/10.3390/su15129846

[7] Roopchund R (2021) Cellulose nanocrystals: plant design for up-scaled production and applications in green construction materials," PhD, Chemical Engineering, University of KwaZulu-Natal, Howard College. [Online]. Available: https://researchspace.ukzn.ac.za/bitstream/handle/10413/20356/Roopchund_Rishen_2021.pdf

[8] Rovnaník P, Šafránková K (2016) Thermal behaviour of metakaolin/fly ash geopolymers with chamotte aggregate. Materials 9(7):535

[9] Javed U, Shaikh FUA, Sarker PK (2024) Thermal stability and strength degradation of lithium slag geopolymer containing fly ash and silica fume. Constr Build Mater 425:135976. https://doi.org/10.1016/j.conbuildmat.2024.135976

[10] Wang R, Zhou X, Zhang W, Ye J, Wang J (2024) Transport mechanism of uranyl nitrate in nanopore of geopolymer with different Si/Al ratios: molecular dynamics simulation. J Solid State Chem 331:124542

[11] Diab MA (2022) Enhancing class F fly ash geopolymer concrete performance using lime and steam curing. J Eng Appl Sci 69(1):59. https://doi.org/10.1186/s44147-022-00111-6

[12] Saludung A, Azeyanagi T, Ogawa Y, Kawai K (2023) Mechanical and microstructural evolutions of fly ash/slag-based geopolymer at high temperatures: effect of curing conditions. Ceram Int 49(2):2091–2101. https://doi.org/10.1016/j.ceramint.2022.09.175

[13] Roopchund R, Andrew J, Sithole B (2023) Using a systematic review to develop a cellulose nanocrystals production framework for use as a design baseline and optimization tool. S Afr J Chem Eng 44:345–355

[14] Rickard WD, Riessen AV, Walls P (2010) Thermal character of geopolymers synthesized from class F fly ash containing high concentrations of iron and α-quartz. Int J Appl Ceramic Technol 7(1):81–88

[15] Rosas-Casarez CA et al (2014) Experimental study of XRD, FTIR and TGA techniques in geopolymeric materials. Int J Adv Comput Sci Appl 4(4):221–226

[16] Caballero LR, Paiva MD, Fairbairn ED, Toledo Filho RD (2019) Thermal, mechanical and microstructural analysis of metakaolin based geopolymers. Mater Res 22(02):e20180716

[17] Lemougna PN et al (2020) Thermal stability of one-part metakaolin geopolymer composites containing high volume of spodumene tailings and glass wool. Cement Concr Compos 114:103792

[18] He R, Dai N, Wang Z (2020) Thermal and mechanical properties of geopolymers exposed to high temperature: a literature review. Adv Civil Eng 2020(1):7532703

[19] Zhao J, Wang K, Wang S, Wang Z, Yang Z, Shumuye ED, Gong X (2021) Effect of elevated temperature on mechanical properties of high-volume fly ash-based geopolymer concrete, mortar and paste cured at room temperature. Polymers 13(9):1473. https://doi.org/10.3390/polym13091473

[20] Liu W, Ju S (2024) Tunable thermal conductivity of sustainable geopolymers by the Si/Al ratio and moisture content: insights from atomistic simulations. J Phys Chem B 128(12):2972–2984. https://doi.org/10.1021/acs.jpcb.3c07445

[21] Pulidori E et al (2025) Thermal behavior of Sicilian clay-based geopolymers. J Ther Anal Calorimet 150(9):6663–6675. https://doi.org/10.1007/s10973-024-13226-0

[22] Xie Y, Wang C, Guo Y, Cui H, Xue J (2025) Improved mechanical and thermal properties of sustainable ultra-high performance geopolymer concrete with cellulose nanofibres. J Build Eng 102:112068. https://doi.org/10.1016/j.jobe.2025.112068

[23] Yildirim N, Shaler S (2017) A study on thermal and nano-mechanical performance of cellulose nanomaterials (CNs). Materials 10(7):718. https://doi.org/10.3390/ma10070718

[24] Liu Y, Wei Y, He Y, Qian Y, Wang C, Chen G (2023) Large-scale preparation of carboxylated cellulose nanocrystals and their application for stabilizing pickering emulsions. ACS Omega 8(17):15114–15123. https://doi.org/10.1021/acsomega.2c08239

[25] Motloung MP, Zungu S, Ojijo V, Bandyopadhyay J, Ray SS (2020) Morphological, thermal, and thermomechanical

properties of cellulose nanocrystals reinforced polylactide/poly [(butylene succinate)-co-adipate] blend composite foams. Funct Compos Mater 1(1):8. https://doi.org/10.1186/s42252-020-00011-z

[26] Alzoubi HH, Albiss BA (2020) Performance of cementitious composites with nano PCMs and cellulose nano fibers. Constr Build Mater 10(236):117483. https://doi.org/10.1016/j.conbuildmat.2019.117483

[27] Liu W, Qin L, Zhao CY, Ju S (2023) Microscopic mechanism of tunable thermal conductivity in carbon nanotube-geopolymer nanocomposites. J Phys Chem B 127(10):2267–2276. https://doi.org/10.1021/acs.jpcb.2c08962

[28] Tran NP, Nguyen TN, Black JR, Ngo TD (2024) High-temperature stability of ambient-cured one-part alkali-activated materials incorporating graphene nanoplatelets for thermal energy storage. Dev Built Environ 18:100447

[29] He Y, Liu L, He L, Cui X (2016) Characterization of chemosynthetic H_3PO_4–Al_2O_3–$2SiO_2$ geopolymers. Ceram Int 42(9):10908–10912

[30] Cao Y et al (2015) The influence of cellulose nanocrystals on the microstructure of cement paste. Cement Concr Compos 74:164–173

[31] Cao Y, Zavattieri P, Youngblood J, Moon R, Weiss J (2016) The relationship between cellulose nanocrystal dispersion and strength. Constr Build Mater 119:71–79

[32] Lee H-J, Kim S-K, Lee H-S, Kim W (2019) A study on the drying shrinkage and mechanical properties of fiber reinforced cement composites using cellulose nanocrystals. Int J Concr Struct Mater 13:1–11

[33] Graytee A, Sanjayan JG, Nazari A (2018) Development of a high strength fly ash-based geopolymer in short time by using microwave curing. Ceram Int 44(7):8216–8222

[34] Kastiukas G, Ruan S, Liang S, Zhou X (2020) Development of precast geopolymer concrete via oven and microwave radiation curing with an environmental assessment. J Clean Prod 255:120290

[35] Rawlinson C (2006) "Differential scanning calorimetry “cooking with chemicals. Poisons, Pills Potions

[36] Yildirim N, Shaler S (2017) A study on thermal and nano-mechanical performance of cellulose nanomaterials (CNs). Materials 10(7):718

[37] Ansar EN, Biutty MN, Kim KS, Yoo S, Huh P, Yoo SI (2024) Sustainable polyamide composites reinforced with nanocellulose via melt mixing process. J Compos Sci. 8(10):419. https://doi.org/10.3390/jcs8100419

[38] Nasir M et al (2022) Engineered cellulose nanocrystals-based cement mortar from office paper waste: flow, strength, microstructure, and thermal properties. J Build Eng 51:104345. https://doi.org/10.1016/j.jobe.2022.104345